


Anatomy of linear and nonlinear intermolecular exchange in $S = 1$ nanographene

J. C. G. Henriques^{1,2} and J. Fernández-Rossier^{1,*}

¹International Iberian Nanotechnology Laboratory (INL), Av. Mestre José Veiga, 4715-330 Braga, Portugal

²Universidad de Santiago de Compostela, 15782 Santiago de Compostela, Spain

 (Received 17 July 2023; revised 7 September 2023; accepted 28 September 2023; published 20 October 2023)

Nanographene triangulenes with an $S = 1$ ground state have been used as building blocks of topological antiferromagnetic Haldane spin chains. Using inelastic electron spectroscopy, it was found that the intermolecular exchange was described by the bilinear-biquadratic Hamiltonian. Starting from a Hubbard model, we analytically derive these effective spin interactions using perturbation theory, up to fourth order. For chains with more than two units, other interactions arise that entail second neighbor linear and three-site nonlinear exchange. We discuss the extension to general $S = 1$ molecules and give numerical results for the strength of the nonlinear exchange for several nanographenes.

DOI: [10.1103/PhysRevB.108.155423](https://doi.org/10.1103/PhysRevB.108.155423)

I. INTRODUCTION

Nonlinear exchange, i.e., spin interactions that go beyond the simple Heisenberg coupling between two spins, play a prominent role in many physical systems, such as antiferromagnetic transition metal oxides [1], magnetic impurities in insulators [2], magnetic multilayers [3,4], chiral magnets [5], and magnetic two-dimensional materials [6]. Nonlinear exchange is a key ingredient in the exactly solvable Affleck-Kennedy-Lieb-Tasaki (AKLT) models [7], whose ground state is a resource for measurement based quantum computing [8].

The relative size and sign of linear and nonlinear exchange can have a dramatic impact in several contexts. For instance, whereas the swap gate, or permutation operator, for spin qubits can be implemented with a linear Heisenberg interaction [9], for spin qudits it requires the presence of nonlinear exchange terms [10]. Alternatively, in the case of the two-dimensional $S = 3/2$ honeycomb lattice, the relative size of linear and nonlinear exchange controls the nature of the ground state and its excitation spectrum [7,11–13].

Here we undertake the exploration of nonlinear exchange in $S = 1$ nanographenes. This class of system features outstanding flexibility to realize $S = 1$ molecules with different shapes and sizes. It has been recently shown [14] that there are 383 different nanographenes that can be formed with nine hexagons or less. Therefore this type of system provides an ideal arena to engineer intermolecular exchange. One of the simplest $S = 1$ nanographenes is the so-called [3]-triangulene.

Triangulenes are graphene fragments with the shape of an equilateral triangle, of various sizes and terminated with zigzag edges; these are customarily defined in terms of the number of benzenes n in a given edge [15,16] (termed a $[n]$ -triangulene). Based on Lieb's theorem for the Hubbard model for bipartite lattices at half-filling [17], $[n]$ -triangulenes are predicted to be open-shell multiradicals, with the spin of the ground state scaling as $2S = n - 1$, associated with a half-full shell of $n - 1$ in-gap nonbonding zero modes [15,18–22].

Due to recent breakthroughs in bottom-up synthesis techniques [16,23–26], and the capability of atomic precision manipulation of organic molecules, triangulenes have been used as building blocks of larger molecular structures [27–30]. A prime example of this is the recent realization of Haldane spin chains, where [3]-triangulenes (henceforth referred simply as triangulene) were coupled in order to generate chains with more than 16 units [28]. There, the inelastic electron tunneling spectroscopy (IETS) was described with an effective $S = 1$ spin Hamiltonian that included both linear and nonlinear exchange terms, i.e., the so called BLBQ Hamiltonian [31–35]:

$$H_{\text{BLBQ}} = \sum_i JS_i \cdot S_{i+1} + B(S_i \cdot S_{i+1})^2, \quad (1)$$

where each triangulene is represented by a spin-1 operator S_i , the sum runs over all triangulenes in the chain and the parameters J and B are the linear and nonlinear exchange couplings, respectively. The introduction of the nonlinear exchange term proved essential to increase the accuracy of the spin model when compared with experimental data [28] and full fermionic numerical approaches [33].

In the following, we derive the effective $S = 1$ spin Hamiltonian (1) starting from a fermionic model for the nanographenes. Importantly, our derivation unveils the presence of additional second neighbor linear interactions, and nonlinear exchange that involve three-spin terms, with strength comparable to B in Eq. (1). The rest of this paper is organized as follows. In Sec. II, we introduce the fermionic

*On permanent leave from Departamento de Física Aplicada, Universidad de Alicante, 03690 San Vicente del Raspeig, Spain.

model that is used to describe nanographenes. We focus particularly on triangulenes as a prototypical example, and discuss the modification that are required to study other $S = 1$ nanographenes. In Sec. III, using perturbation theory up to fourth order order we derive the effective spin Hamiltonian for triangulene chains. For the case with more than two triangulenes, we obtain new terms in the spin Hamiltonian which were neglected in other BLBQ-based approaches. In Sec. IV, we discuss the possibility of engineering the exchange interactions in the effective spin model by considering other $S = 1$ nanographenes as building blocks. At last, in Sec. V, we give a summary of our results and discuss possible future studies on this type of system. Four Appendixes close the paper.

II. MODEL

A. Hubbard Hamiltonian

As a fermionic model we use a single-orbital Hubbard Hamiltonian (considering only p_z orbitals at the carbon sites) at half-filling, containing hoppings between first (t) and third neighbor (t_3) sites and an on-site Hubbard repulsion term (U) which deals with the intra-atomic Coulomb repulsion cost associated with having a given π -orbital doubly occupied [22]. Explicitly,

$$H_{\text{Hubb.}} = t \sum_{(i,j)} \sum_{\sigma} c_{i,\sigma}^{\dagger} c_{j,\sigma} + t_3 \sum_{\langle\langle(i,j)\rangle\rangle} \sum_{\sigma} c_{i,\sigma}^{\dagger} c_{j,\sigma} + U \sum_i n_{i\uparrow} n_{i\downarrow}, \quad (2)$$

where $\langle \dots \rangle$ and $\langle\langle \dots \rangle\rangle$ refer to sums over first and third neighbors, respectively; the operator $c_{i,\sigma}^{(\dagger)}$ annihilates (creates) an electron at site- i with spin $\sigma = \uparrow, \downarrow$ and $n_{i,\sigma} = c_{i,\sigma}^{\dagger} c_{i,\sigma}$. The second neighbor hopping is neglected here as it breaks electron-hole symmetry, which leads to an inhomogeneous distribution of the charge [36], that is counterbalanced by long-range Coulomb interactions. As a result, fitting tight-binding models to *ab-initio* calculations leads to a second-neighbour hopping 5 times smaller than third-neighbour hopping [37], and is often neglected [38]. Recent theoretical and experimental work [39] shows the prominent role played by third-neighbour hopping in the intermolecular exchange of $S = 1/2$ triangulenes. The Hubbard model has been validated by comparison with multiconfigurational calculations obtained with full-quantum chemistry *ab initio* methods [22], for $t = -2.7$ eV, $t_3 \sim t/10$ and $U \sim |t|$ [40]. *Ab initio* calculations often yield larger estimates for U than the one we are considering [41], likely due to the neglect of screening effects from a conducting substrate (something that must be accounted for when comparing theoretical predictions with experimental data).

B. Single-particle energies

At the single-particle level, i.e., taking $U = 0$ in Eq. (2), the Hamiltonian can be solved exactly. As mentioned in the introduction, for triangulenes, as well as other $S = 1$ nanographenes, the single-particle spectrum features two in gap nonbonding zero modes, localized in the majority sublattice of the nanographene [22]. Let us now consider the case

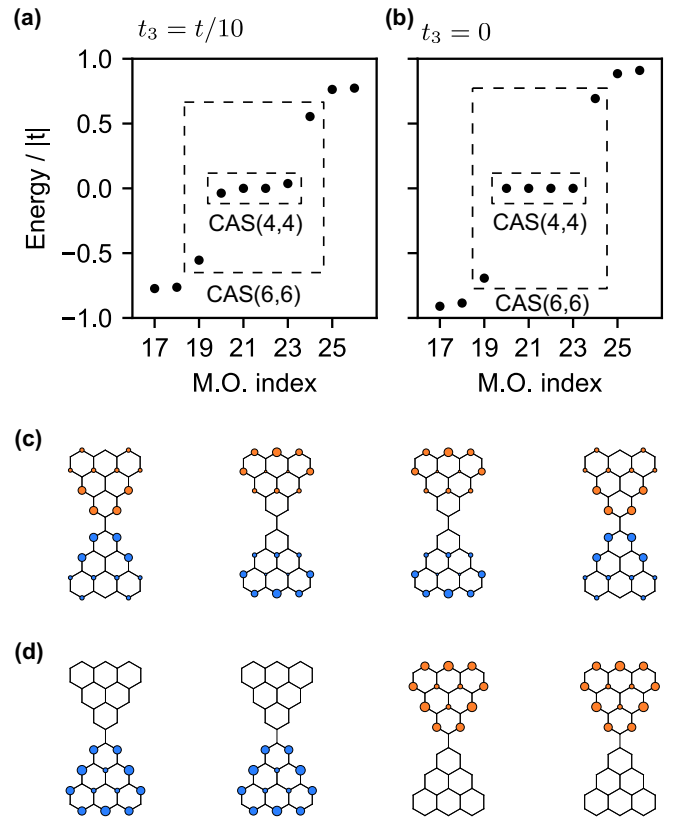


FIG. 1. Single-particle energies for the triangulene dimer with $t_3 = t/10$ (a) and 0 (b). Energies are given in unit of $|t| = 2.7$ eV. The dashed boxes indicate two possible choices for the active space where the Hubbard Hamiltonian is represented. CAS(N_o, N_e) refers to an active space with N_o modes where N_e electrons are distributed. (c) and (d) show the absolute value of the site representation of the four molecular orbitals closer to zero energy for $t_3 = t/10$ and 0, respectively. Each circle is colored according to the sublattice where it is located.

where two triangulenes are coupled, forming a dimer. The results for the single-particle spectrum, as well as the wave functions of the zero modes, for $t_3 = 0$ and $t_3 \neq 0$ are depicted in Fig. 1. When $t_3 = 0$, we find that the dimer has four degenerate zero modes, two per triangulene. This is a direct consequence of the lack of intermolecular hybridization, since first neighbor hopping connects the two triangulenes via their minority sublattices only, thus preventing the hybridization of the two pairs of zero modes (since the respective wave functions have no weight on the minority sublattice). Due to the degeneracy of these 4 modes, there is some freedom in how their wave functions are defined. We represent them as eigenfunctions of the C_3 symmetry operator with eigenvalues $\pm 2\pi/3$. For future reference we refer to these modes as the C_3 symmetric basis.

Turning on t_3 , we observe that the previously degenerate zero modes are now slightly split. This is due to the intermolecular hybridization of the two sets of zero modes which is now made possible by t_3 , since this hopping parameter connects the two triangulenes via their majority sublattices. This hybridization is also clear in the representation of the wave functions which now show the typical bonding and

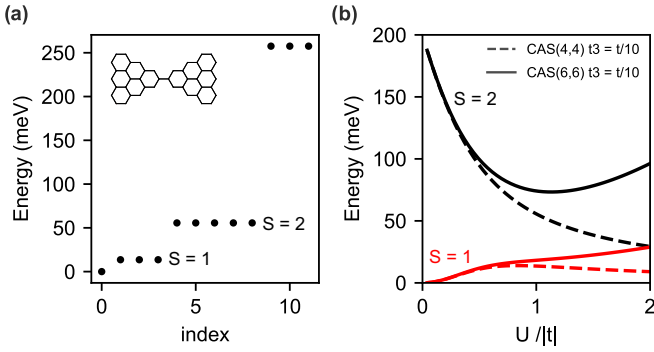


FIG. 2. (a) Eigenvalues of the Hubbard Hamiltonian for the triangulene dimer obtained with CAS(4,4), with $U = |t|$, $t_3 = t/10$, and $t = -2.7$ eV. (b) Energy of the first two excited manifolds (triplet in red, and quintuplet in black) as a function of U obtained with CAS(4,4) (dashed) and CAS(6,6) (solid).

antibonding structure of hybridized modes. This is the molecular orbital basis. Although our analysis of the single-particle spectrum focused on triangulene dimers, similar analysis with identical results can be performed for larger chains as well as other $S = 1$ molecules.

C. CAS

Contrarily to the single-particle problem, the Hubbard Hamiltonian with interactions, i.e. $U \neq 0$, can only be numerically diagonalized exactly for rather smaller systems due to the exponential increase of the Hilbert space as the system size grows. For the molecules we presently wish to discuss, the Hubbard model with finite U can only be solved using approximate approaches. Here, we make use of the configuration interaction approach combined with the complete active space (CAS) approximation [22]. In this framework, the single-particle problem is solved first. Then, the full Hamiltonian is expressed in terms of the single-particle eigenstates, and N_e electrons are distributed over a subset of N_O orbital close to zero energy; the remaining electrons fully occupy the orbitals at lower energy (at charge neutrality, $N_e = N_O$). Considering once again the triangulene dimer, we solve the Hubbard Hamiltonian at charge neutrality in an active space composed of the four zero modes only, i.e. CAS(4,4), and obtain the results depicted in Fig. 2(a). In agreement with Lieb's theorem [17] and owing to the lack of sublattice imbalance of the dimer, the ground state is a singlet. The first two excited manifolds are a triplet, followed by a quintuplet. At higher energies, well separated from these low energy excitations, other manifolds appear. In panel (b), we plot the energy of the first two excited states (the triplet in red and the quintuplet in black) as a function of U , obtained with CAS(4,4) and CAS(6,6) calculations, where in the latter an additional pair of orbitals is accounted for. There, we find that in the parameter region we are considering the energies are already well described by the CAS(4,4) calculation; including an additional pair of orbitals unlocks the Coulomb driven exchange mechanism [42] which introduces an additional correction to the energies.

The low energy part of this energy spectrum, i.e., a singlet followed by a triplet and then a quintuplet, clearly resembles

the energy levels of two antiferromagnetically coupled spin 1 and prompts us to obtain an effective spin model for this type of system.

D. Hamiltonian in the basis of zero modes

The first step in the derivation of an effective spin Hamiltonian is to represent the Hamiltonian in the C_3 symmetric basis taking into account only the four modes at zero energy. The representation of the Hubbard model in that basis leads to the following effective Hamiltonian:

$$\begin{aligned}
 H = & \sum_{\mu'\mu} \sum_{\sigma} \tau_{\mu'\mu} d_{\mu',\sigma}^{\dagger} d_{\mu,\sigma} + \sum_{\mu} \mathcal{U}_{\mu} n_{\mu,\uparrow} n_{\mu,\downarrow} \\
 & + \sum_{\Delta} \mathcal{J}_{\Delta_+, \Delta_-} (n_{\Delta_+, \uparrow} n_{\Delta_-, \downarrow} + n_{\Delta_-, \uparrow} n_{\Delta_+, \downarrow}) \\
 & + \sum_{\Delta} \mathcal{J}_{\Delta_+, \Delta_-} (d_{\Delta_+, \uparrow}^{\dagger} d_{\Delta_-, \uparrow}^{\dagger} d_{\Delta_-, \downarrow}^{\dagger} d_{\Delta_+, \downarrow}^{\dagger} + \text{H.c.}), \quad (3)
 \end{aligned}$$

where μ and μ' run over the four C_3 symmetric modes and $\sigma = \uparrow, \downarrow$. The sums over Δ run over the two triangulenes, and Δ_{\pm} refers to the modes with eigenvalues $\pm 2\pi/3$ in a given triangulene. The operator $d_{\mu,\sigma}^{\dagger}$ annihilates (creates) an electron in the μ mode with spin σ , and $n_{\mu,\sigma} = d_{\mu,\sigma}^{\dagger} d_{\mu,\sigma}$.

This Hamiltonian contains three distinct types of terms. The first term in Eq. (3) represents the hopping between two modes, μ and μ' , with an amplitude $\tau_{\mu\mu'} = t_3 \sum_{\langle\langle(i,j)\rangle\rangle} \Phi_{\mu}^*(i) \Phi_{\mu'}(j)$ where $\Phi_{\mu}(i)$ is the site representation of the μ mode (depicted in Fig. 1). This hopping amplitude is zero when the two modes are localized in the same sublattice; thus, hoppings between modes in the same triangulene vanish. In addition, due to the C_3 symmetry of the μ modes, all the finite hoppings have the same absolute value, which we label simply as τ .

The remaining terms in the Hamiltonian account for electron-electron interactions. The second term of Eq. (3), corresponds to an effective Hubbard repulsion that penalizes the double occupancy of a given mode μ , with the energy penalty being given by the inverse participation ratio [43] (IPR) times the Hubbard repulsion U , and is defined as $\mathcal{U}_{\mu} = U \sum_i |\Phi_{\mu}(i)|^4$, where the sum runs over all the sites; the IPR is a metric of the delocalization of a given wave function. Again, due to the C_3 symmetry of the modes, one finds $\mathcal{U}_{\mu} \equiv \mathcal{U}$ is independent of μ .

The last two lines in Eq. (3) describe an intra-triangulene ferromagnetic exchange interaction, with the exchange coupling given by $\mathcal{J}_{\mu\mu'} = U \sum_i |\Phi_{\mu}(i)|^2 |\Phi_{\mu'}(i)|^2$. As before, $\mathcal{J}_{\mu\mu'} = \mathcal{J}$ is independent of μ and μ' , and $\mathcal{U} = \mathcal{J}$.

Therefore the model (3) realizes a Creutz-ladder [44], with the difference that the vertical hoppings are replaced by a ferromagnetic exchange and there are Hubbard interactions. In Fig. 3, we present a pictorial representation of the Hamiltonian of Eq. (3) for the triangulene dimer, as well as the extension to larger structures, e.g., a triangulene chain. The extension of Eq. (3) to triangulene chains is easily obtained by running the sums over all triangulenes.

Let us note in passing, that for molecules less symmetric than triangulenes, for example panels (c) to (f) of Fig. 5, the hoppings $\tau_{\mu\mu'}$, the effective Hubbard repulsion \mathcal{U}_{μ} , and

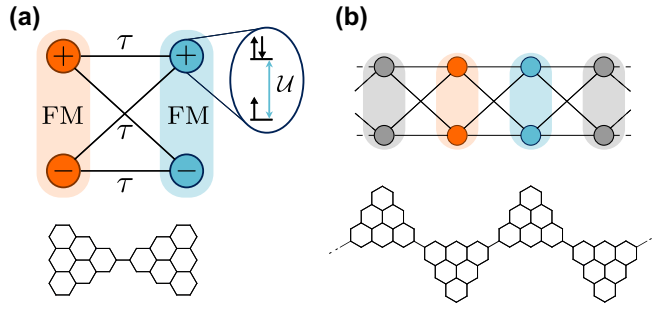


FIG. 3. (a) Schematic representation of the interactions present in the Hamiltonian of Eq. (3), with modes in the same triangulene ferromagnetically coupled, and hoppings between the two triangulenes. (b) Extension of the model for the case of a triangulene chain.

the exchange coupling $\mathcal{J}_{\mu\nu}$ are in principle mode-dependent. Moreover, it might be necessary to include a new term associated with electron-pair hoppings in Eq. (3). As discussed in [22], this term vanishes for triangulenes, but may be finite for other molecules. Including it is straightforward, and does not affect the main physical features we presently wish to discuss.

III. EFFECTIVE SPIN MODEL

Starting from the many-body fermionic model just presented in Eq. (3), we now produce an effective low energy description which can be related to the effective spin model. To this end, we shall employ degenerate perturbation up to fourth order, treating the hoppings τ as a perturbation (for $U \sim t$ we have $U/\tau \sim 5$). An alternative approach to determine linear and nonlinear exchange, based on the so-called magnetic force theorem [45] has recently been used in the study of triangulene spin chains [46].

A. Dimer

For the unperturbed system ($\tau = 0$) the two pairs of modes are decoupled, and each triangulene can be studied individually. At half-filling, with two electrons per triangulene, the lowest energy states in a given triangulene are $|\uparrow\rangle|\uparrow\rangle$, $|\downarrow\rangle|\downarrow\rangle$

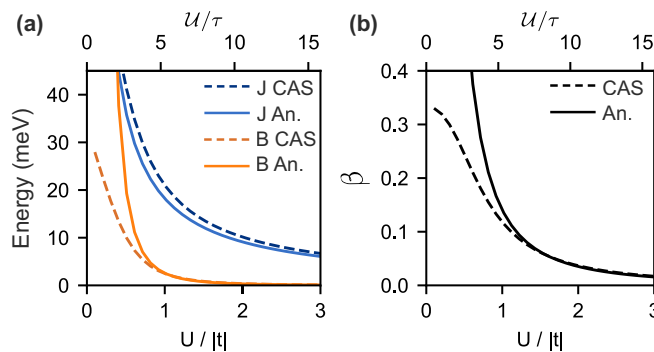


FIG. 4. Comparison between the analytical expression and the result found from numerical diagonalization for (a) the linear exchange J and the nonlinear exchange B , and (b) the ratio $\beta = B/J$ as a function of the on-site Hubbard repulsion U in units of $|t| = 2.7$ eV with $t_3 = t/10$.

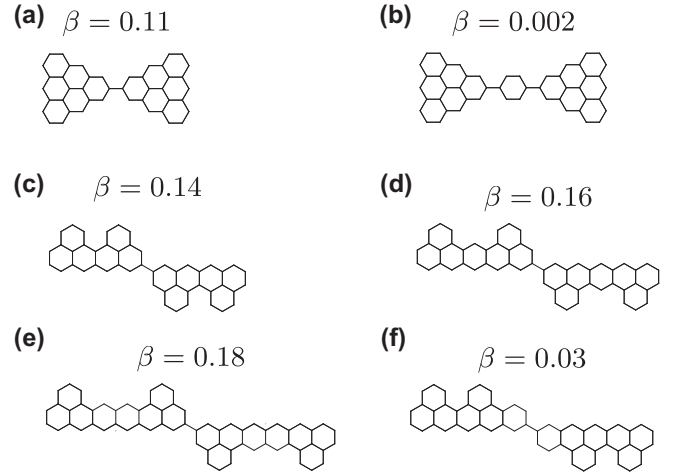


FIG. 5. Values obtained for $\beta = B/J$ by numerically diagonalizing the Hubbard Hamiltonian in a restricted Hilbert space with 4 modes only, for dimers obtained from $S = 1$ building blocks, taking $U = |t|$, $t_3 = t/10$, and $|t| = 2.7$ eV.

and $(|\uparrow\rangle|\downarrow\rangle + |\downarrow\rangle|\uparrow\rangle)/\sqrt{2}$, where each ket refers to one of the C_3 symmetric modes in a triangulene. These states correspond to the three spin projections of an $S = 1$ state formed by the ferromagnetic coupling of two spin-1/2 electrons, i.e., $|\uparrow\rangle|\uparrow\rangle \equiv |\uparrow\rangle$, $|\downarrow\rangle|\downarrow\rangle \equiv |\downarrow\rangle$ and $(|\uparrow\rangle|\downarrow\rangle + |\downarrow\rangle|\uparrow\rangle)/\sqrt{2} \equiv |+\rangle$, with the ket on the right hand side referring to the state of the triangulene as a whole. With these three states in each triangulene, the total unperturbed dimer Hamiltonian at half-filling is nine-fold degenerate. From the CAS numerical solution given in Fig. 2, one sees that the low energy spectrum is composed of 9 states as well, i.e. a singlet, a triplet and a quintuplet. Hence, we expect that as we allow τ to increase, the nine-fold degenerate manifold will split, and a spin model shall emerge.

Representing Eq. (1) in the basis of two spin-1 objects, and focusing on the $S_z = 0$ sector, one finds that while the bilinear term, proportional to J , is responsible for connecting the state $|+\rangle|+\rangle$ with the states $|\uparrow\rangle|\downarrow\rangle$ and $|\downarrow\rangle|\uparrow\rangle$, the biquadratic term, proportional to B , unlocks a new interaction between the states $|\uparrow\rangle|\downarrow\rangle$ and $|\downarrow\rangle|\uparrow\rangle$ (see Appendix A for details). Recalling the definition of the spin-1 states in terms of two spin-1/2, one realizes that while the processes mediated by J link states which differ by two spin flips, the process mediated by B connects states differing by four spin flips. Hence, the biquadratic interaction is only to be expected in fourth-order perturbation theory, while the bilinear term should already be present in 2nd order.

The expressions for the second- and fourth-order corrections in degenerate perturbation theory read [47,48]

$$h_{kp}^{(2)} = \sum_m \frac{\langle k|H_\tau|m\rangle\langle m|H_\tau|p\rangle}{\Delta E_m^{(0)}}, \quad (4)$$

$$h_{kp}^{(4)} = \sum_{mm'm''} \frac{\langle k|H_\tau|m\rangle\langle m|H_\tau|m'\rangle\langle m'|H_\tau|m''\rangle\langle m''|H_\tau|p\rangle}{\Delta E_m^{(0)}\Delta E_{m'}^{(0)}\Delta E_{m''}^{(0)}} - \sum_{mm'l} \frac{\langle k|H_\tau|m\rangle\langle m|H_\tau|l\rangle\langle l|H_\tau|m'\rangle\langle m'|H_\tau|p\rangle}{\Delta E_m^{(0)}\Delta E_{m'}^{(0)}\Delta E_{m''}^{(0)}}, \quad (5)$$

where k , p , and l label states inside the degenerate ground state, and the sums run over all the states outside that subspace. The perturbation is $H_\tau = \sum_{\mu\mu'} \sum_\sigma \tau_{\mu\mu'} d_{\mu\sigma}^\dagger d_{\mu'\sigma}$ and $\Delta E_m^{(0)}$ is the unperturbed energy of the $|m\rangle$ state relative to the ground state. In the absence of applied magnetic field, the odd-order corrections vanish identically [49]. One important aspect to note is that even though the initial and final states correspond to open-shell configurations with two electrons per triangulene, the intermediate states contain closed-shell configurations, as well as charge excitations, with different number of electrons in the two triangulenes.

In second-order perturbation theory, where only two electron flips are considered, a finite contribution for J is found, which for the present system simply reads:

$$J^{(2)} = 2 \frac{\tau^2}{U}. \quad (6)$$

This result is similar to the one usually found when a Hubbard chain is mapped to a Heisenberg chain of antiferromagnetically coupled spins; the different numerical pre-factor stemming from the different geometry of our system.

Progressing to 4th order perturbation theory, where processes involving up to four electron are considered, different paths appear which allow for $|\uparrow\rangle|\downarrow\rangle \rightarrow |\downarrow\rangle|\uparrow\rangle$. Carrying out the necessary calculations, one finds that finite contributions appear for both J and B . These are given by

$$J^{(4)} = 4 \frac{\tau^4}{U^3} \quad B^{(4)} = 8 \frac{\tau^4}{U^3}. \quad (7)$$

The second-order contribution to J dominates its fourth-order counterpart in the physically relevant region of the parameter space, and $J^{(4)}$ may be neglected. Hence, combining the results from second and fourth order perturbation theory, we find in leading order:

$$J \approx \frac{2\tau^2}{U}, \quad B \approx \frac{8\tau^4}{U^3}, \quad \beta \equiv \frac{B}{J} \approx \frac{4\tau^2}{U^2}. \quad (8)$$

Using the definitions of τ [40] and U [22], and assuming $t_3 \approx t/10$, one can estimate the strength of the quadratic exchange with respect to the linear one, characterized by β , using $\beta \approx 0.1(t/U)^2$. This rough approximation yields a nice agreement with the value $\beta = 0.09$ that was found in the description of experimental data in Ref. [28]. This good agreement, together with the analytical expressions of Eq. (8), indicate that nonlinear exchange is a higher order manifestation of the same underlying kinetic exchange mechanism [1] that gives rise to linear exchange.

To validate our analytical expressions we shall now compare them with the results found from numerical diagonalization. The numerical results are obtained by first diagonalizing Eq. (3), followed by matching the energies of the first excitations with those of the spin Hamiltonian. This gives numerically both J and B as a function of the parameters of the microscopic model, U and t_3 , and allows the comparison with Eq. (8).

In Fig. 4, we show the comparison between the analytical expressions found for J and B and the numerical results. Inspecting this figure reveals an excellent agreement between the two approaches, especially in the region $U \gg |t|$ where perturbation theory is valid. Crucially, this agreement holds

near $U \sim |t|$, the physically relevant region. For $U = |t|$, one finds the linear exchange $J = 20$ meV and $\beta = 0.11$. As U increases β approaches 0, and a Heisenberg-like picture is recovered. For $U \ll |t|$, outside the validity region of perturbation theory, the mapping to a spin model fails since the order of low energy excitations is no longer the same in the two approaches [35]. The fact that β is bounded by the AKLT limit $\beta = 1/3$ is a consequence of Lieb's theorem, which prevents a four-fold degenerate ground state. As we shall see later in the text, using different $S = 1$ molecules as building blocks it is possible to modify the strength of nonlinear exchange.

B. Larger chains

Having completed the study of the triangulene dimer, we extend our analysis to chains with more than two triangulenes. The analysis is identical, although more convoluted, to the one we just performed for the dimer, and as a result we refer the reader to Appendix A for details. Generalizing Eq. (3) to include more triangulenes, and once again employing perturbation theory up to fourth order, we find that for a chain composed of N triangulenes the effective spin Hamiltonian reads

$$H_N = J \sum_{i=1}^{N-1} \mathbf{S}_i \cdot \mathbf{S}_{i+1} + B \sum_{i=1}^{N-1} (\mathbf{S}_i \cdot \mathbf{S}_{i+1})^2 + J_2 \sum_{i=1}^{N-2} \mathbf{S}_i \cdot \mathbf{S}_{i+2} + B_{1,1} \sum_{i=1}^{N-2} (\mathbf{S}_i \cdot \mathbf{S}_{i+1})(\mathbf{S}_{i+1} \cdot \mathbf{S}_{i+2}) + \text{H.c.} \quad (9)$$

While the first line corresponds to the BLBQ model for N triangulenes, the second and third lines contain new exchange interactions; the former describes an antiferromagnetic second neighbor linear exchange, and the latter a ferromagnetic quadratic exchange involving two adjacent triangulene pairs. We note that the antiferromagnetic second neighbor linear exchange might promote frustration if its strength becomes comparable with J . If perturbation theory is extended up to sixth or eighth order, additional exchange interactions appear; however, since these are in higher order of τ/U , we neglect their contribution. Crucially, the terms proportional to J_2 and $B_{1,1}$ appear in the same order of perturbation theory as B and therefore must be accounted for. To leading order, we find the following analytical expressions for the parameters of the spin model:

$$J = \frac{2\tau^2}{U}, \quad B = \frac{8\tau^4}{U^3}, \quad J_2 = \frac{79\tau^4}{12U^3}, \quad B_{1,1} = -\frac{37\tau^4}{12U^3}. \quad (10)$$

In Appendix B, we benchmark the effective spin model of Eq. (9) and the analytical expression for the model parameters against CAS calculations of the Hubbard model for the case of a triangulene trimer. We find a very good agreement that supports the validity of the analytical results. In the same Appendix, we also compare the spin model with the exact numerical diagonalization of a four-site model trimer, thus allowing us to rule out the possibility that the new exchange interactions are artifacts arising from the restriction of the Hilbert space. Considering all this, a consistent description of triangulene spin chains should include these terms, missing in previous analysis [28].

As a preliminary study of the effect of these new terms in the Hamiltonian, in Appendix C, we study $S = 1$ chains and rings with up to $L = 13$ spins. Using exact diagonalization (with the QUSPIN package [50,51]), we compute the singlet and triplet splitting (i.e., the energy of the first excitation) of the spin chains as a function of the chain length L for both the BLBQ Hamiltonian and Eq. (9). A similar procedure is applied to the rings, where the energy of the first excitation converges to the Haldane gap in the limit of $L \gg 1$. There, one finds that the two models share the same qualitative features, although quantitatively some differences appear. We have verified that the Haldane gap, as determined from the $L = 13$ with PBC, interpolates smoothly as we deform the Hamiltonian from the BLBQ limit to the new Hamiltonian, without ever closing. Therefore the new terms do not induce a topological phase transition. An interesting prospect for future works would be to study in detail how these new interactions, as well as higher order ones we neglected in the present discussion, would affect the phase diagram of the spin model, using, for example, density matrix renormalization group (DMRG) approaches.

IV. ENGINEERING OF EXCHANGE

We now briefly explore the nonlinear exchange of various $S = 1$ dimers. By applying numerical diagonalization in the minimal CAS, and comparing it with the excitation energies of the BLBQ Hamiltonian, we obtain the value of β for different dimers composed of molecules with a triplet ground state. This should predict the relevance of nonlinear exchange, as well as its tunability, in chains formed with different building blocks.

In Fig. 5(b), we show a triangulene dimer, where a benzene ring is introduced as a spacer between the two triangulenes. Formally, this molecule is nearly identical to the dimer we considered in the text [depicted in panel (a)], with the main difference being that due to the extra benzene, intermolecular hybridization between the two triangulenes is greatly diminished, resulting in a smaller τ . This leads to $\beta = 0.002$, two orders of magnitude smaller than what we found for the case without the spacer. As discussed in Appendix D, CAS(4,4) underestimates the value of β for this dimer due to the larger role played by Coulomb driven exchange [42].

Next, we consider the molecule of panel (c), where each monomer is composed of two Phenalenyl side-by-side; for this dimer $\beta = 0.14$. As benzenes are added between the two Phenalenyl, depicted in panels (d) [52] and (e), the value of β increases to $\beta = 0.16$ and $\beta = 0.18$, respectively. This increase in β may be ascribed to the decrease of the IPR of the zero modes of the individual molecules, i.e., the increased delocalization of the wave functions. At last, we consider panel (f), where an additional benzene is added close to the binding site of the two molecules. This leads to a significant decrease of β to $\beta = 0.03$. The reason for this sharp decrease is similar to the one we gave when discussing panel (b). Hence, we see that by carefully choosing the geometry of the molecules used as building blocks, it should be possible to engineer the strength of nonlinear exchange.

Even though we restricted our analysis to the minimal CAS, accounting only for the zero modes, additional orbitals

could have been included in the calculation (see Fig. 1). This would introduce the so-called Coulomb driven superexchange discussed in Ref. [42]. We have verified that including this additional mechanism would slightly change the numerical results, but preserve the qualitative features of the model.

V. SUMMARY

We have considered chains of $S = 1$ nanographenes, taking the case of triangulene chains [28,29] as the prototypical example. Using perturbation theory we have found that nonlinear exchange interactions are a higher order manifestation of the same mechanisms that give rise to linear exchange, and we have obtained analytical expressions for their amplitude. The analytical results permit us to relate molecule geometry with β , the degree of exchange nonlinearity. In addition, our analysis for chains with more than two molecules shows that new terms appear in the Hamiltonian, namely a second neighbor linear and a three-site non linear exchange interaction, going beyond the BLBQ paradigm. Future work will address the impact of these extra terms on the well established phase diagram of the BLBQ model.

ACKNOWLEDGMENT

We acknowledge fruitful discussions with Gonalo Catarina, Ant3nio Costa, and David Jacob. We acknowledge financial support from FCT (Grant No. PTDC/FIS-MAC/2045/2021), SNF Sinergia (Grant Pimag), FEDER/Junta de Andaluc3a (Grant No. P18-FR-4834), Generalitat Valenciana funding Prometeo2021/017 and MFA/2022/045, and funding from MICIIN-Spain (Grant No. PID2019-307 109539GB-C41).

APPENDIX A: DERIVATION OF THE EFFECTIVE SPIN HAMILTONIAN

1. Triangulene dimer

In this Appendix, we describe in more detail how to obtain the BLBQ Hamiltonian, given in the main text, for a triangulene dimer using perturbation theory. As discussed in the main text, the unperturbed Hamiltonian ($\tau = 0$) for the triangulene dimer has a nine-fold degenerate ground state. Since the perturbation conserves S_z we focus our analysis in a single S_z sector, $S_z = 0$. There are three states with $S_z = 0$ in the degenerate ground state manifold, namely $|\uparrow\rangle|\downarrow\rangle$, $|\downarrow\rangle|\uparrow\rangle$ and $|+\rangle|+\rangle$ where each ket refers to a triangulene, and $|\uparrow\rangle = |\uparrow\rangle|\uparrow\rangle$, $|\downarrow\rangle = |\downarrow\rangle|\downarrow\rangle$ and $|+\rangle = (1/\sqrt{2})(|\uparrow\rangle|\downarrow\rangle + |\downarrow\rangle|\uparrow\rangle)$ where each ket on the right hand side refers to one of the two C_3 symmetric modes in a given triangulene. Using the equation given in the main text for the second-order correction to the Hamiltonian, and computing the matrix elements using the aforementioned three states with $S_z = 0$, one finds:

$$h^{(2)} = \frac{\tau^2}{\mathcal{U}} \begin{bmatrix} -4 & 2 & 0 \\ 2 & -2 & 2 \\ 0 & 2 & -4 \end{bmatrix}, \quad (\text{A1})$$

where the matrix is represented in the basis $|\uparrow\rangle|\downarrow\rangle$, $|+\rangle|+\rangle$, $|\downarrow\rangle|\uparrow\rangle$. At this point we note in passing that when

performing this type of calculation one should be careful with the sign conventions in the definitions of the fermionic states. Representing the BLBQ Hamiltonian in the same basis, we find

$$h_{\text{BLBQ}} = \begin{bmatrix} -J + 2B & J - B & B \\ J - B & 2B & J - B \\ B & J - B & -J + 2B \end{bmatrix}. \quad (\text{A2})$$

Demanding the two Hamiltonian to be equal (apart from some constant energy shift), we find the second-order contribution to J and B to be given by

$$J^{(2)} = 2\frac{\tau^2}{\mathcal{U}}, \quad B^{(2)} = 0, \quad (\text{A3})$$

as obtained in the main text. In order to find the fourth-order corrections to J and B a similar procedure is followed. Using the expression given in the main text for $h_{kp}^{(4)}$, we arrive at

$$h^{(4)} = \frac{\tau^4}{\mathcal{U}^3} \begin{bmatrix} 0 & -4 & 8 \\ -4 & 4 & -4 \\ 8 & -4 & 0 \end{bmatrix}. \quad (\text{A4})$$

Once again, using the matrix representation of the BLBQ Hamiltonian as a reference, we obtain

$$J^{(4)} = 4\frac{\tau^4}{\mathcal{U}^3}, \quad B^{(4)} = 8\frac{\tau^4}{\mathcal{U}^3}. \quad (\text{A5})$$

As mentioned in the main text, because $J^{(4)}$ is of higher order in τ/\mathcal{U} than $J^{(2)}$, its contribution is rather small, and can be safely neglected. To better illustrate this let us consider

some typical values for τ and \mathcal{U} . For triangulenes, one has $\tau = 2t_3/11$ and $\mathcal{U} \approx 0.1U$. Taking $U = |t|$ and $t_3 = t/10$ as typical values, we find $J^{(4)}/J^{(2)} = 2\tau^2/\mathcal{U}^2 \approx 0.06$, which makes $J^{(4)}$ more than one order of magnitude smaller than $J^{(2)}$.

2. Extension to larger chains

We now extend the results of the previous section to larger triangulene chains. We restrict our analysis to the chain with three triangulenes, a trimer, which already hosts the interactions which are absent in the dimer. For the triangulene trimer the ground state of the unperturbed system is a $3^3 = 27$ degenerate manifold. Of these, seven states belong to the $S_z = 0$ subspace. These seven states are the ones we will consider in the following analysis. Using the definition of $h^{(2)}$ given in the main text, and considering the basis $|\uparrow\rangle|\uparrow\rangle|\downarrow\rangle$, $|\uparrow\rangle|\downarrow\rangle|\uparrow\rangle$, $|\uparrow\rangle|\uparrow\rangle|\downarrow\rangle$, $|\uparrow\rangle|\uparrow\rangle|\uparrow\rangle$, $|\uparrow\rangle|\downarrow\rangle|\uparrow\rangle$, $|\downarrow\rangle|\uparrow\rangle|\uparrow\rangle$, $|\downarrow\rangle|\uparrow\rangle|\uparrow\rangle$, we find

$$h^{(2)} = \frac{\tau^2}{\mathcal{U}} \begin{bmatrix} -4 & 2 & 2 & 0 & 0 & 0 & 0 \\ 2 & -6 & 0 & 2 & 0 & 0 & 0 \\ 2 & 0 & -6 & 2 & 0 & 0 & 0 \\ 0 & 2 & 2 & -4 & 2 & 2 & 0 \\ 0 & 0 & 0 & 2 & -6 & 0 & 2 \\ 0 & 0 & 0 & 2 & 0 & -6 & 2 \\ 0 & 0 & 0 & 0 & 2 & 2 & -4 \end{bmatrix}. \quad (\text{A6})$$

In the same basis, the BLBQ Hamiltonian reads

$$h_{\text{BLBQ}} = \begin{bmatrix} 2B & J & J & 0 & 0 & 0 & 0 \\ J & 3B - J & 0 & J - B & 0 & B & 0 \\ J & 0 & 3B - J & J - B & B & 0 & 0 \\ 0 & J - B & J - B & 4B & J - B & J - B & 0 \\ 0 & 0 & B & J - B & 3B - J & 0 & J \\ 0 & B & 0 & J - B & 0 & 3B - J & J \\ 0 & 0 & 0 & 0 & J & J & 2B \end{bmatrix}. \quad (\text{A7})$$

Once again demanding the two Hamiltonian to be equal apart from a constant shift in energy we find

$$J^{(2)} = 2\frac{\tau^2}{\mathcal{U}}, \quad B^{(2)} = 0. \quad (\text{A8})$$

Extending this analysis to fourth order, we find for $h^{(4)}$:

$$h^{(4)} = \frac{\tau^4}{12\mathcal{U}^3} \begin{bmatrix} -182 & 86 & 86 & 5 & 0 & 0 & 0 \\ 86 & -56 & -74 & -47 & 42 & 96 & 0 \\ 86 & -74 & -56 & -47 & 96 & 42 & 0 \\ 5 & -47 & -47 & 89 & -47 & -47 & 5 \\ 0 & 42 & 96 & -47 & -56 & -74 & 86 \\ 0 & 96 & 42 & -47 & -74 & -56 & 86 \\ 0 & 0 & 0 & 5 & 86 & 86 & -182 \end{bmatrix}. \quad (\text{A9})$$

Comparing this matrix with h_{BLBQ} it is clear that some entries which vanish in h_{BLBQ} are finite in $h^{(4)}$; this clearly indicates that the BLBQ model is incomplete, and additional interactions should be accounted for in order to describe the triangulene trimer with an effective spin model. To determine

which interactions are lacking, one should study which states yield a finite matrix element in $h^{(4)}$ that is not captured by the BLBQ Hamiltonian. For example, the states $|\uparrow\rangle|\uparrow\rangle|\downarrow\rangle$ and $|\uparrow\rangle|\uparrow\rangle|\uparrow\rangle$ give a finite matrix element in $h^{(4)}$. These two states are clearly connected via a second neighbor linear

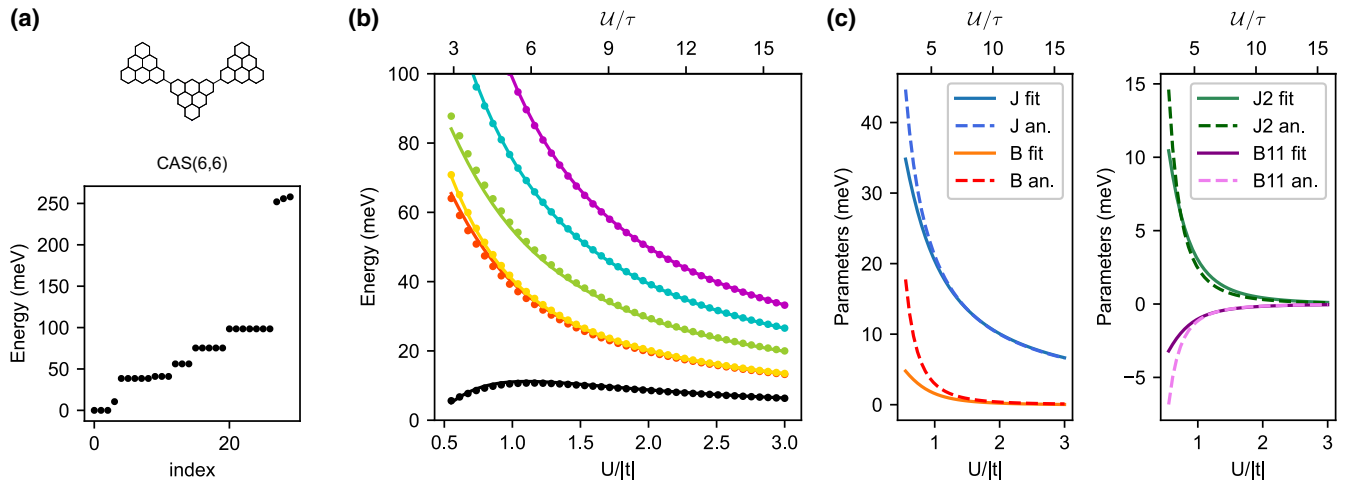


FIG. 6. (a) Energies obtained from CAS(6,6) for the triangulene trimer with $U = |t|$ and $t_3 = t/10$. (b) Comparison between the first six excitation energies obtained by solving the Hubbard model for the triangulene trimer with CAS(6,6) with $t_3 = t/10$ (dots) and the ones obtained by fitting the spin model to the CAS results (lines). (c) Comparison between the parameters of the spin model obtained from fitting to CAS with the analytical expressions obtained with perturbation theory.

exchange which links the first and third triangulenes, i.e., $\mathbf{S}_1 \cdot \mathbf{S}_3$, and produces the spin flip $|\uparrow\rangle|\dots\rangle|\downarrow\rangle \rightarrow |+\rangle|\dots\rangle|+\rangle$. Applying the same type of reasoning to the other matrix elements that are not properly captured by the BLBQ model, we find that the appropriate spin Hamiltonian to describe the trimer up to fourth order in τ/U reads

$$\begin{aligned}
 H = & J(\mathbf{S}_1 \cdot \mathbf{S}_2 + \mathbf{S}_2 \cdot \mathbf{S}_3) + B[(\mathbf{S}_1 \cdot \mathbf{S}_2)^2 + (\mathbf{S}_2 \cdot \mathbf{S}_3)^2] \\
 & + J_2 \mathbf{S}_1 \cdot \mathbf{S}_3 + B_{1,1}[(\mathbf{S}_1 \cdot \mathbf{S}_2)(\mathbf{S}_2 \cdot \mathbf{S}_3) \\
 & + (\mathbf{S}_2 \cdot \mathbf{S}_3)(\mathbf{S}_1 \cdot \mathbf{S}_2)]
 \end{aligned} \quad (\text{A10})$$

with the fourth-order corrections to the coefficients being given by

$$\begin{aligned}
 J^{(4)} &= \frac{49}{12} \frac{\tau^4}{U^3}, \quad B^{(4)} = 8 \frac{\tau^4}{U^3}, \quad J_2^{(4)} = \frac{79}{12} \frac{\tau^4}{U^3}, \\
 B_{1,1}^{(4)} &= -\frac{37}{12} \frac{\tau^4}{U^3}.
 \end{aligned} \quad (\text{A11})$$

Notice that while $B^{(4)}$ is the same that we found in the dimer, $J^{(4)}$ differs from the one we found before by $\tau^4/12U^3$; we thus see that the presence of an additional triangulene slightly renormalizes the linear exchange between nearest neighbors. This is due to processes with four electron hoppings, where an electron visits the third triangulene, but leaves without changing its initial state. If we applied the procedure we described so far to higher order corrections in perturbation theory, new interactions would once again appear in the Hamiltonian. An example of this is the second neighbor biquadratic exchange $(\mathbf{S}_1 \cdot \mathbf{S}_3)^2$. These new interactions, however, would produce minute changes in the effective description of the trimer, and as a result, we drop them. In Appendix B, we shall compare the energies obtained by fitting the eigenvalues of Eq. (A10) to the many-body energies of the triangulene trimer obtained with CAS(6,6) (anticipating the results presented there, the agreement is excellent). The extension to even larger chains can be obtained in a straightforward manner using the procedure we just described. Doing so, gives

similar results, up to fourth order, to what we obtained for the trimer.

APPENDIX B: COMPARISON BETWEEN SPIN MODEL AND HUBBARD MODEL FOR TRIMERS

1. Triangulene trimer

In this Appendix, we briefly discuss how we numerically validate the analytical results found with perturbation theory for the triangulene trimer. In Fig. 6(a), we plot the energies obtained with CAS(6,6), whose active space contains only the zero modes (two in each triangulene), for the triangulene trimer. There, we see that the ground state is a triplet, followed by several low energy excitations, which are well separated by a gap from other high energy states. Regarding the spin model, we found that the model Hamiltonian has four parameters, J , B , J_2 , and $B_{1,1}$. Contrarily to the case of the dimer discussed in the main text, the low energy spectrum of the trimer has more excitation energies than there are parameters in the spin model (this is a consequence of truncating the effective spin model at 4th order). Thus, it is not possible to write a linear system of equations which relates the parameters of the spin model with the CAS excitation energies. Instead, we obtain the dependence of the parameters with U and t_3 by fitting the eigenenergies of the spin model to the first 3^3 states from CAS [like the ones of Fig. 6(a)] taking the parameters of the spin model as fitting parameters. The parameters so obtained can then be compared with the analytical expressions, testing their validity. In Fig. 6(b), we compare the energies obtained by fitting the spin model to the CAS calculation for different values of U and fixed $t_3 = t/10$.

The agreement between the two approaches is clear, and it validates the spin model proposed by us. In panel (c) of the same figure, we show the comparison between J , B , J_2 and $B_{1,1}$ obtained from the fitting procedure and the analytical ones. Once again, the two data sets show an excellent agreement. Next, we shall study a similar system where the

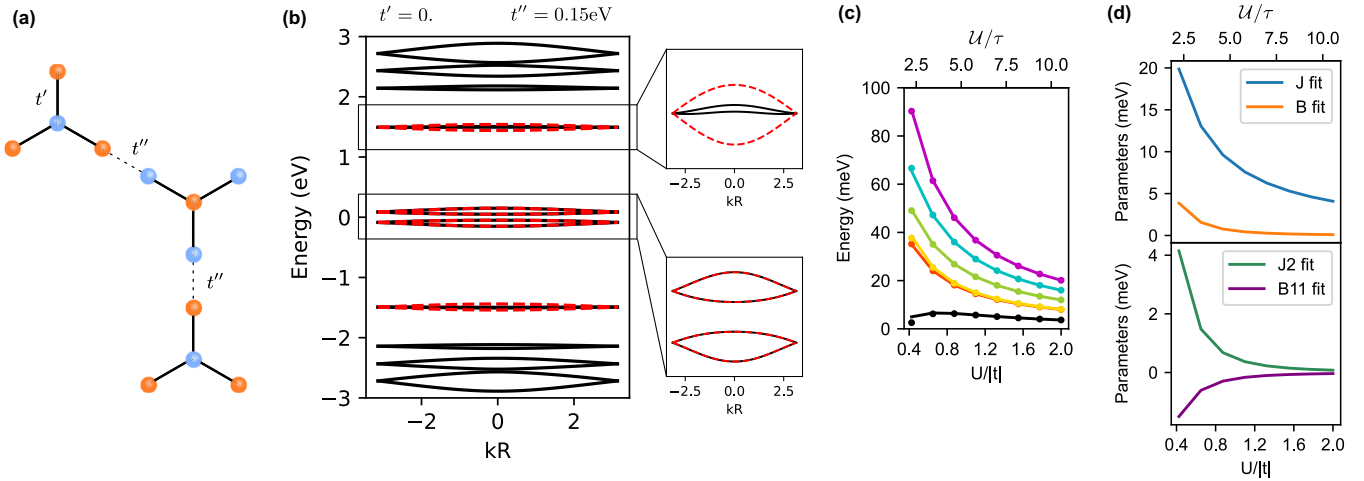


FIG. 7. (a) Schematic representation of a four-site model trimer. (b) Bands obtained for an infinite triangulene chain (solid black lines) with $t = -2.7$ eV and $t_3 = t/10$, and for a chain of four-site models (red dashed lines) obtained with $t' = -0.86$ eV and $t'' = -0.15$ eV. (c) Comparison between the excitation energies obtained with exact diagonalization of the Hubbard model and the energies obtained from the spin Hamiltonian fit. (d) Parameters of the spin model obtained from the fitting procedure.

triangulenes are substituted by a simplified system, allowing us to use solve the Hubbard model exactly.

2. Four-site model

Let us now benchmark the effective spin Hamiltonian against the Hubbard model for a four-site model trimer [depicted in Fig. 7(a)] instead of the complete triangulene trimer. The four-site model (i.e., the building block) has been successfully used in the past to emulate triangulenes, since its sublattice imbalance and C_3 symmetry endows this system with main properties of a [3]triangulene [28,33]. The fundamental advantage of this simplified model is that, due to its reduced number of sites, exact diagonalization can be used (we use the QuSpin package [50,51] to perform the diagonalization). This should allow us to rule out the possibility that the spin interactions present in the model we proposed are spurious artifacts stemming from the constraints imposed in the active space. The values of the hoppings t' and t'' [see Fig. 7(a)] are determined by computing the bands of an infinite chain [40], and fitting them to the bands of a triangulene chain with $t = -2.7$ eV and $t_3 = t/10$. In Fig. 7(b), we depict the comparison between the bands of the two chains, obtained for $t' = -0.86$ eV and $t'' = -0.15$ eV. With the parameters of the four-site model fixed, we compute the energies for the trimer via exact diagonalization. Then, we fit the spin model to the first 3^3 states obtained from exact diagonalization. In Fig. 7(c), we show the fit of the energies to the ones obtained with exact diagonalization; an excellent agreement is observed. In panel (d) of the same figure, we show the parameters of the spin model obtained from the fitting procedure; the signs and relative magnitudes are similar to those we just obtained for the triangulene trimer. This confirms that the interactions that appear in the model we derived are not artifacts caused by the restriction of the Hilbert space in the CAS approximation.

APPENDIX C: EXACT DIAGONALIZATION OF SPIN CHAINS AND RINGS

In this Appendix, we wish to compare the BLBQ Hamiltonian with the complete Hamiltonian given in Eq. (9), and infer the possible effects of the exchange interactions which are absent in the BLBQ model. To achieve this, we shall exactly diagonalize (using the QUSPIN package [50,51]) the two spin models for spin chains with up to $L = 13$ $S = 1$ spins; we consider both open boundary conditions (OBC) as well as periodic boundary conditions (PBC), thus realizing spin rings.

In Fig. 8(a), we consider the case with OBC, and depict the evolution of the singlet-triplet splitting (i.e., the energy of the first excitation) as a function of the chain length L . For both models we find that the singlet-triplet splitting decays exponentially. Assuming that this energy splitting takes the form $Ae^{-L/\xi}$, with A some constant and ξ the correlation length, we obtain $\xi \sim 2$ and $\xi \sim 3$ when Eq. (9) and the BLBQ model are considered, respectively.

In Fig. 8(b), we focus on the case with PBC, i.e. spin rings, and track the evolution of the first excitation as a function of the chain length; in the limit $L \gg 1$ this should converge to the Haldane gap. Due to computational limitations we are unable to go beyond 13 spins, and consequently we do not accurately capture the saturation of the first excitation energy. Nonetheless, it is clear that the results for both model share the same qualitative features, and appear to only differ on the Haldane gap, which is larger when the Hamiltonian of Eq. (9) is used.

Hence, with this simple analysis we see that in region of the parameter space we are considering, which is the relevant one for this kind of system, the new interactions that appear in Eq. (9), and are absent in the BLBQ model, preserve the qualitative features of the spin model, although quantitatively some differences appear. Future studies

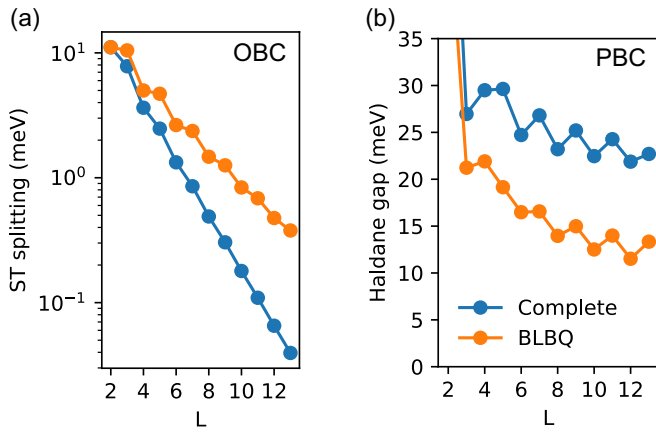


FIG. 8. (a) Singlet-triplet spinning (i.e., energy of the first excitation) obtained for $S = 1$ spin chains with up to 13 spins considering open boundary conditions. (b) Energy of the first excitation for spin chains with periodic boundary conditions, i.e., spin rings. In both panels, the exact diagonalization was applied considering the complete Hamiltonian of Eq. (9) and the BLBQ Hamiltonian. The parameters were determined using Eq. (10) and considering $t = -2.7$ eV, $t_3 = t/10$ and $U = |t|$, i.e., $J = 20$ meV, $B_1 = 2.97$ meV, $J_2 = 2.45$ meV, and $B_{1,1} = -1.14$ meV (the last two parameters are only used in the complete model).

should focus on a more thorough comparison of the two models.

APPENDIX D: THE EFFECT OF INCREASING THE ACTIVE SPACE ON THE VALUE OF β

At last, in this Appendix, we perform a more detailed study on the values of β for the $S = 1$ dimers discussed in the final part of the main text. We shall compute both J and B for several values of U in two different active spaces, i.e. CAS(4,4) which accounts only for the 4 zero modes, and CAS(6,6) which includes the highest occupied molecular orbital and the lowest unoccupied molecular orbital. In the CAS(4,4) calculation, we use $t_3 = t/10$, while in the CAS(6,6) calculation, we consider $t_3 = 0$. In the relevant region of the parameter space, i.e., $U \sim |t|$ the different exchange mechanisms are additive, and the results for CAS(6,6) with $t_3 = t/10$ are essentially given by summing the results from CAS(4,4) with $t_3 = t/10$ with the ones from CAS(6,6) with $t_3 = 0$ [42]. These results are summarized in Fig. 9; in Table I we show the corresponding value of β obtained for $U = |t|$ with the two considered active spaces with $t_3 = t/10$. From Table I, we see that the values of β obtained with CAS(4,4) and CAS(6,6) are similar in all cases, except for the triangulene dimer separated with a benzene, i.e., case (b). For this particular molecule, the

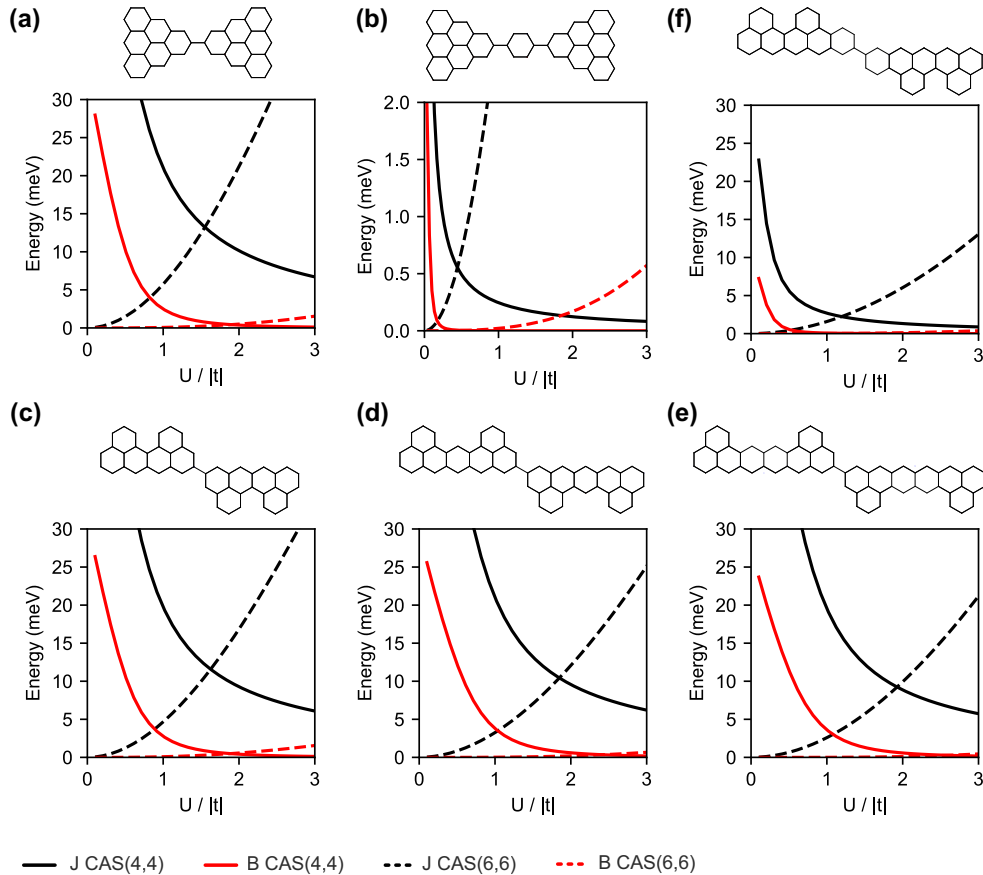


FIG. 9. Values for J (black) and B (red) as a function of U obtained by comparing the BLBQ spectrum with CAS calculations for the six dimers shown in the main text. Solid lines represent results obtained from CAS(4,4) with $t_3 = t/10$ and dashed lines correspond to results obtained with CAS(6,6) with $t_3 = 0$.

TABLE I. Values of $\beta = B/J$ obtained by comparing the BLBQ energies with CAS(4,4) and CAS(6,6) calculations, with $U = |t|$ and $t_3 = t/10$, for the six molecules mentioned in the main text.

	a	b	c	d	e	f
$\beta_{\text{CAS}(4,4)}$	0.11	0.002	0.14	0.16	0.18	0.03
$\beta_{\text{CAS}(6,6)}$	0.11	0.01	0.14	0.16	0.16	0.03

benzene that separates the two triangulenes leads to a substantial reduction of intermolecular hybridization, as can be seen in Fig. 9 where the values of J and B are one order of

magnitude smaller than the ones of case (a) where the benzene spacer is absent. Due to the very weak intermolecular hybridization of the zero modes, the contribution from CAS(4,4) is not enough to accurately describe the system in the region $U \sim |t|$, and processes involving orbitals higher/lower in energy must be accounted for, as evidenced by the difference between CAS(4,4) and CAS(6,6) calculations. Regarding the remaining molecules depicted in Fig. 9, we note that the contribution to exchange coming from CAS(4,4) is the most relevant one for $U \sim |t|$. However, as U increases, the contribution from Coulomb driven exchange becomes more relevant and can even surpass the one coming from the hybridization of zero modes.

- [1] P. W. Anderson, *Phys. Rev.* **115**, 2 (1959).
- [2] E. Harris and J. Owen, *Phys. Rev. Lett.* **11**, 9 (1963).
- [3] J. C. Slonczewski, *Phys. Rev. Lett.* **67**, 3172 (1991).
- [4] P. Mellado, [arXiv:2307.01133](https://arxiv.org/abs/2307.01133) [cond-mat.str-el].
- [5] S. Paul, S. Haldar, S. Von Malotki, and S. Heinze, *Nat. Commun.* **11**, 4756 (2020).
- [6] A. Kartsev, M. Augustin, R. F. Evans, K. S. Novoselov, and E. J. Santos, *npj Comput. Mater.* **6**, 150 (2020).
- [7] I. Affleck, T. Kennedy, E. H. Lieb, and H. Tasaki, *Phys. Rev. Lett.* **59**, 799 (1987).
- [8] T.-C. Wei, I. Affleck, and R. Raussendorf, *Phys. Rev. Lett.* **106**, 070501 (2011).
- [9] D. P. DiVincenzo, D. Bacon, J. Kempe, G. Burkard, and K. B. Whaley, *Nature (London)* **408**, 339 (2000).
- [10] P. H. Segraves, Representation of Permutation Operator in Quantum Mechanics, Master's thesis, University of British Columbia, 1964.
- [11] R. Ganesh, D. N. Sheng, Y.-J. Kim, and A. Paramekanti, *Phys. Rev. B* **83**, 144414 (2011).
- [12] M. Koch-Janusz, D. I. Khomskii, and E. Sela, *Phys. Rev. Lett.* **114**, 247204 (2015).
- [13] N. Pomata and T.-C. Wei, *Phys. Rev. Lett.* **124**, 177203 (2020).
- [14] Y. Yan, F. Zheng, B. Qie, J. Lu, H. Jiang, Z. Zhu, and Q. Sun, *J. Phys. Chem. Lett.* **14**, 3193 (2023).
- [15] J. Fernández-Rossier and J. J. Palacios, *Phys. Rev. Lett.* **99**, 177204 (2007).
- [16] J. Su, M. Telychko, S. Song, and J. Lu, *Angew. Chem., Int. Ed.* **59**, 7658 (2020).
- [17] E. H. Lieb, *Phys. Rev. Lett.* **62**, 1201 (1989).
- [18] A. A. Ovchinnikov, *Theor. Chim. Acta* **47**, 297 (1978).
- [19] W. L. Wang, S. Meng, and E. Kaxiras, *Nano Lett.* **8**, 241 (2008).
- [20] W. L. Wang, O. V. Yazyev, S. Meng, and E. Kaxiras, *Phys. Rev. Lett.* **102**, 157201 (2009).
- [21] O. V. Yazyev, *Rep. Prog. Phys.* **73**, 056501 (2010).
- [22] R. Ortiz, R. Á. Boto, N. García-Martínez, J. C. Sancho-García, M. Melle-Franco, and J. Fernández-Rossier, *Nano Lett.* **19**, 5991 (2019).
- [23] P. Ruffieux, S. Wang, B. Yang, C. Sánchez-Sánchez, J. Liu, T. Dienel, L. Talirz, P. Shinde, C. A. Pignedoli, D. Passerone *et al.*, *Nature (London)* **531**, 489 (2016).
- [24] S. Mishra, D. Beyer, K. Eimre, J. Liu, R. Berger, O. Groning, C. A. Pignedoli, K. Müllen, R. Fasel, X. Feng *et al.*, *J. Am. Chem. Soc.* **141**, 10621 (2019).
- [25] J. Su, M. Telychko, P. Hu, G. Macam, P. Mutombo, H. Zhang, Y. Bao, F. Cheng, Z.-Q. Huang, Z. Qiu *et al.*, *Sci. Adv.* **5**, eaav7717 (2019).
- [26] S. Mishra, K. Xu, K. Eimre, H. Komber, J. Ma, C. A. Pignedoli, R. Fasel, X. Feng, and P. Ruffieux, *Nanoscale* **13**, 1624 (2021).
- [27] S. Mishra, D. Beyer, K. Eimre, R. Ortiz, J. Fernández-Rossier, R. Berger, O. Gröning, C. A. Pignedoli, R. Fasel, X. Feng and P. Ruffieux, Collective all-carbon magnetism in triangulene dimers, *Angewandte Chemie* **132**, 12139 (2020).
- [28] S. Mishra, G. Catarina, F. Wu, R. Ortiz, D. Jacob, K. Eimre, J. Ma, C. A. Pignedoli, X. Feng, P. Ruffieux *et al.*, *Nature (London)* **598**, 287 (2021).
- [29] J. Hieulle, S. Castro, N. Friedrich, A. Vegliante, F. R. Lara, S. Sanz, D. Rey, M. Corso, T. Frederiksen, J. I. Pascual *et al.*, *Angew. Chem., Int. Ed.* **60**, 25224 (2021).
- [30] S. Cheng, Z. Xue, C. Li, Y. Liu, L. Xiang, Y. Ke, K. Yan, S. Wang, and P. Yu, *Nat. Commun.* **13**, 1705 (2022).
- [31] K. Tanaka, Y. Yokoyama, and C. Hotta, *J. Phys. Soc. Jpn.* **87**, 023702 (2018).
- [32] W.-J. Hu, S.-S. Gong, H.-H. Lai, Q. Si, and E. Dagotto, *Phys. Rev. B* **101**, 014421 (2020).
- [33] G. Catarina and J. Fernández-Rossier, *Phys. Rev. B* **105**, L081116 (2022).
- [34] R. Soni, N. Kaushal, C. Şen, F. A. Reboredo, A. Moreo, and E. Dagotto, *New J. Phys.* **24**, 073014 (2022).
- [35] G. Catarina, J. C. G. Henriques, A. Molina-Sánchez, A. T. Costa, and J. Fernández-Rossier, [arXiv:2306.17153](https://arxiv.org/abs/2306.17153) [cond-mat.str-el].
- [36] N. M. R. Peres, F. Guinea, and A. H. Castro Neto, *Phys. Rev. B* **73**, 125411 (2006).
- [37] V.-T. Tran, J. Saint-Martin, P. Dollfus, and S. Volz, *AIP Adv.* **7**, 075212 (2017).
- [38] D. Gunlycke and C. T. White, *Phys. Rev. B* **77**, 115116 (2008).
- [39] N. Krane, E. Turco, A. Bernhardt, D. Jacob, G. Gandus, D. Passerone, M. Luisier, M. Juríček, R. Fasel, J. Fernández-Rossier *et al.*, [arXiv:2307.09930](https://arxiv.org/abs/2307.09930).
- [40] R. Ortiz, G. Catarina, and J. Fernández-Rossier, *2D Mater.* **10**, 015015 (2023).
- [41] T. O. Wehling, E. Şaşıoğlu, C. Friedrich, A. I. Lichtenstein, M. I. Katsnelson, and S. Blügel, *Phys. Rev. Lett.* **106**, 236805 (2011).
- [42] D. Jacob and J. Fernández-Rossier, *Phys. Rev. B* **106**, 205405 (2022).
- [43] F. Wegner, *Z. Phys. B* **36**, 209 (1980).

- [44] M. Creutz, *Phys. Rev. Lett.* **83**, 2636 (1999).
- [45] A. I. Liechtenstein, M. Katsnelson, V. Antropov, and V. Gubanov, *J. Magn. Magn. Mater.* **67**, 65 (1987).
- [46] G. Martínez-Carracedo, L. Oroszlány, A. García-Fuente, L. Szunyogh, and J. Ferrer, *Phys. Rev. B* **107**, 035432 (2023).
- [47] C. J. Calzado and J.-P. Malrieu, *Phys. Rev. B* **69**, 094435 (2004).
- [48] J. P. Malrieu, R. Caballol, C. J. Calzado, C. De Graaf, and N. Guihery, *Chem. Rev.* **114**, 429 (2014).
- [49] A. H. MacDonald, S. M. Girvin, and D. Yoshioka, *Phys. Rev. B* **37**, 9753 (1988).
- [50] P. Weinberg and M. Bukov, *SciPost Phys.* **2**, 003 (2017).
- [51] P. Weinberg and M. Bukov, *SciPost Phys.* **7**, 020 (2019).
- [52] X. Su, C. Li, Q. Du, K. Tao, S. Wang, and P. Yu, *Nano Lett.* **20**, 6859 (2020).